JACS
JOURNAL OF THE AMERICAN CHEMICAL SOCIETY
pubs.acs.org/JACS
Article

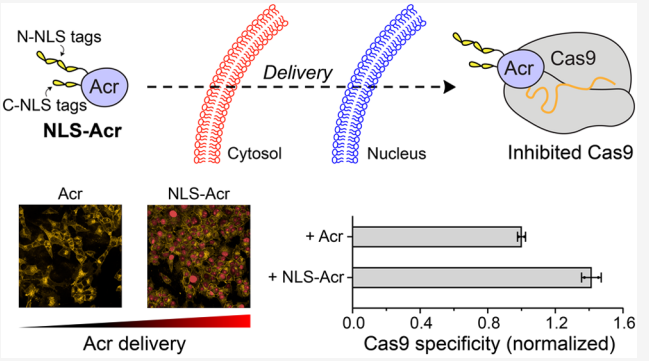
Nuclear Localization Signals Enable the Cellular Delivery of an Anti-CRISPR Protein to Control Genome Editing

Axel O. Vera, Franklin J. Avilés-Vázquez, Taekjip Ha, Amit Choudhary,* and Ronald T. Raines*

Cite This: J. Am. Chem. Soc. 2026, 148, 51200−51211
https://doi.org/10.1021/jacs.5c19089

ACCESS | Metrics & More | Article Recommendations | Supporting Information

ABSTRACT: Precise regulation of Cas9 activity is essential to minimize off-target effects, mosaicism, chromosomal alterations, immunogenicity, and genotoxicity in genome editing. Although type II anti-CRISPR proteins (Acrs) can inhibit and regulate Cas9, their size and anionic charge generally prevent them from crossing the cell membrane. Existing Acr delivery methods employing vectors or electroporation are either slow and persistent or require external equipment, limiting their therapeutic utility. To address these challenges, we developed a cell-permeable Acr (6×NLS-Acr), which uses nuclear localization signals (NLSs) to cross the cell membrane. We conjugated 6×NLS-Acr to a fluorescent dye to elucidate its cellular entry mechanism and directly visualized its binding to a fluorescent Cas9·gRNA complex to study its inhibitory mechanism. 6×NLS-Acr (IC_{50} = 0.47 μM) directly transduces human cells, including immortalized cell lines, embryonic stem cells, and 3D cell cultures, within 5 min, inhibiting up to 99% of Cas9 activity and increasing genome-editing specificity by nearly 100%. We further compared 6×NLS-Acr with our anthrax-derived Acr delivery platform. Our results demonstrate that 6×NLS-Acr is the most efficacious cell-permeable CRISPR-Cas inhibitor, significantly enhancing the precision and therapeutic potential of CRISPR-based genome editing.



INTRODUCTION

Clustered regularly interspaced short palindromic repeats (CRISPR)/CRISPR-associated (Cas) systems use RNA-guided endonucleases (e.g., Cas9) to cleave foreign DNA and defend bacteria against phage infections.[1,2] Due to its ease of programmability, Cas9 has been adapted as a powerful genome-editing tool in human cells.[3,4] Cas9-based technologies are advancing the treatment of genetic disorders,[5−7] but their broader application is hindered by safety concerns, including unintended DNA modifications (i.e., off-target effects),[8−11] genetic mosaicism,[12] chromosomal abnormalities,[13] immunogenicity,[14] and genotoxicity.[15,16]

Type II anti-CRISPR proteins (Acrs) can address these limitations by inhibiting Cas9 in cells. Evolved by phages to disable bacterial CRISPR immunity, Acrs bind Cas9 with high specificity and affinity.[17,18] They inhibit Cas9 at one or more of its three interference stages: gRNA loading, DNA binding, or DNA cleavage.[19] For instance, AcrIIA4, an anionic Acr, predominantly binds to the PAM-interacting domain of the Cas9·gRNA ribonucleoprotein (RNP) complex, thereby preventing DNA binding.[20−22] Acrs have been used to regulate Cas9 activity,[23,24] mitigate its toxicity,[25] and increase its efficiency[26] and specificity.[22,27−31]

Because they cannot cross cell membranes, Acrs require delivery vehicles to enter cells. Viral vectors (e.g., adenovirus,[25] AAVs,[27,28,32] and lentiviruses,[33,34]) and lipid nanoparticles[35] have been used to deliver Acr-encoding DNA and mRNA, ex vivo and in vivo, validating the therapeutic potential of Acrs. Viral vectors, however, require expression, are immunogenic, and can integrate into the host genome.[36] In contrast, mRNA delivery is transient and avoids genomic integration but still relies on cellular translation, which takes time and can be influenced by cell type and stress. Consequently, DNA- and mRNA-based Acr delivery methods are slow, delaying Cas9 inhibition by several hours.[37]

Delivering Acrs directly as proteins via nucleofection could overcome this delay, enabling immediate Cas9 inhibition.[22] As a nonviral method, nucleofection avoids host genome integration, prolonged Acr expression, and vector packaging constraints. Yet, nucleofection requires specialized equipment and electrical pulses, limiting its use to ex vivo applications. Additionally, delivering Cas9 and Acrs sequentially via nucleofection can increase cellular stress and toxicity.[38]

Received: October 29, 2025
Revised: March 28, 2026
Accepted: March 31, 2026
Published: September 4, 2026



ACS Publications
© 2026 The Authors. Published by American Chemical Society

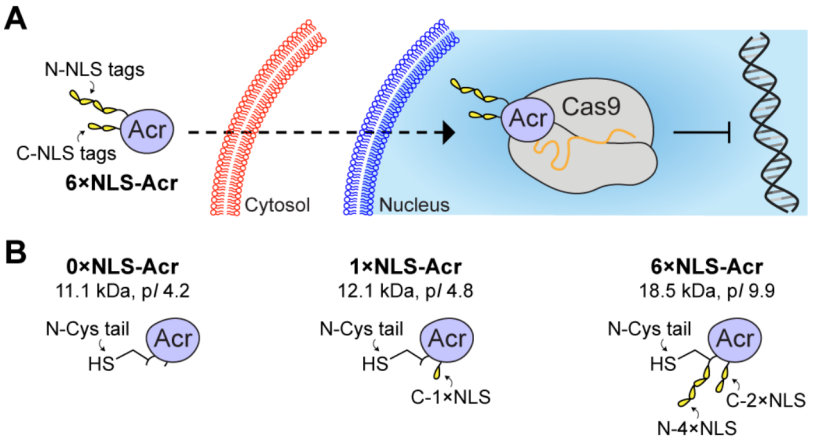


Figure 1. Nuclear localization signals (NLSs) to deliver Acrs into cells. (A) Cationic NLSs deliver Acrs into the cytosol and nucleus of a cell. (B) Cartoon representations of 0×NLS-Acr, 1×NLS-Acr, and 6×NLS-Acr. Acrs were recombinantly produced and purified in *Escherichia coli*. The Acr sequence corresponds to AcrIIA4 from *L. monocytogenes* prophages, engineered with an N-terminal G_4CG_4S sequence (i.e., an N-Cys tail) to facilitate site-specific bioconjugation. Acrs are labeled based on the number (0, 1, or 6×) of SV40 NLSs (sequence: PKKKRKV) inserted at either terminus. The molar mass and isoelectric point (p*I*) of each Acr variant were determined using the Expasy ProtParam tool.

As an alternative to nucleofection, we recently established LF_N-Acr/PA—a protein-based delivery system for introducing Acrs into human cells.[31] LF_N-Acr/PA consists of two proteins derived from anthrax toxin. The first component, LF_N-Acr, is a fusion between the nontoxic N-terminal domain of lethal factor from *Bacillus anthracis* and AcrIIA4 from *Listeria monocytogenes* prophages. The second component, protective antigen (PA) from *B. anthracis*, binds the human receptors ANTRX1 and ANTRX2 and, after protease-mediated activation, forms a pH-triggered endosomal pore that allows LF_N-Acr to enter the cell. LF_N-Acr/PA is the most potent known cell-permeable CRISPR-Cas inhibition system, inhibiting Cas9 at concentrations as low as 2.5 pM and increasing its specificity by up to 40%. The LF_N-Acr/PA system is, however, limited by its reliance on two separate protein components—LF_N-Acr and PA—for Acr delivery. Additionally, PA pore formation requires binding to either the ANTRX1 or ANTRX2 receptor on the cell surface, followed by proteolytic cleavage by a cell-surface furin protease.[39−41] As a result, PA-mediated Acr delivery requires the coordinated action of at least four distinct proteins, further complicating the already intricate process of Cas9 and gRNA delivery.

Here, we describe the first peptide-based delivery system for introducing Acrs into human cells. We show that 6×NLS-Acr, an Acr fused to six nuclear localization signals (NLSs), readily enters cells via a novel direct protein transduction mechanism, inhibits up to 99% of Cas9 activity, and increases genome-editing specificity by 90%. We compare the delivery of 6×NLS-Acr to the PA-mediated delivery of LF_N-Acr. We show that 6×NLS-Acr enters cells less effectively than LF_N-Acr/PA at low concentrations, but more effectively above 1 μM. Unlike LF_N-Acr/PA, 6×NLS-Acr effectively enters cells after Cas9 lipofection. Thus, 6×NLS-Acr is a more efficacious inhibitor, owing to its simpler, one-component, receptor-independent delivery mechanism.

■ RESULTS

Design of the Cellular Delivery System

NLSs are short peptide sequences that transport proteins from the cytosol to the nucleus with the assistance of nuclear import proteins.[42] NLSs (e.g., PKKKRKV, derived from the SV40 antigen) can also function as cell-penetrating peptides (CPPs).[43,44] CPPs can internalize proteins into cells via a combination of mechanisms that include endosomal escape and direct penetration.[45] Tandem arrays (>2) of SV40 NLSs have been used to deliver zinc finger nucleases[46] and Cas proteins (e.g., Cas9 inserted between four N-terminal NLSs and two C-terminal NLSs) into cells.[47−51]

Thus, we hypothesized that NLSs could mediate the cellular delivery of Acrs (Figure 1A). A cell-permeable NLS-Acr fusion would have the advantage of being a nonviral, single-component entity. It would enter cells rapidly (within 1 h) if it behaves like other NLS fusion proteins.[44] Cell-permeable NLS fusion proteins have been shown to penetrate tissues in vivo;[47,50,51] hence, NLS-Acrs could also be applicable in vivo.

We chose AcrIIA4 as a model Acr because it potently inhibits *Streptococcus pyogenes* Cas9 (SpCas9) and tolerates modifications at its termini, including the insertion of dual cysteine residues.[20,52] We first introduced a cysteine residue in the N-terminus of AcrIIA4 to allow site-specific bioconjugation. We then produced and purified Cys-AcrIIA4 without SV40 NLSs (0×NLS-Acr), Cys-AcrIIA4 with a C-terminal SV40 NLS (1×NLS-Acr), and Cys-AcrIIA4 inserted between four N-terminal SV40 NLSs and two C-terminal SV40 NLSs (6×NLS-Acr) using an MBP-TEV system in *E. coli* and assessed purity by SDS−PAGE and LC−MS (Figures 1B and S1−S3). 0×NLS-Acr and 1×NLS-Acr are anionic proteins (p*I* 4.2−4.8), whereas 6×NLS-Acr is a cationic protein (p*I* 9.9). Their masses range from 11.1 to 18.5 kDa.

6×NLS-Acr Inhibits Cas9 in a Dose- and Time-Dependent Manner with High Specificity

We tested Acr delivery by monitoring Cas9 nuclease activity using the *GFP*-disruption assay. We delivered Cas9 RNP targeting a *GFP* gene via nucleofection into a cell line stably expressing a GFP−PEST fusion (U2OS-EGFP.PEST).[53] We then treated the seeded cells with Acrs at time points ranging from 0 to 24 h and imaged at 48 h. Cas9-mediated cleavage of *GFP* reduces GFP fluorescence. Conversely, Acr-mediated inhibition of Cas9 conserves GFP fluorescence (Figure 2A). 6×NLS-Acr (0.13−4 μM) inhibited Cas9 activity (always normalized to 100% without Acrs) from 100 to 4.9% (Figures 2B,2C, and S4−S9). 0×NLS-Acr (4 μM) and 1×NLS-Acr (4

https://doi.org/10.1021/jacs.5c19089
J. Am. Chem. Soc. 2026, 148, 51200−51211

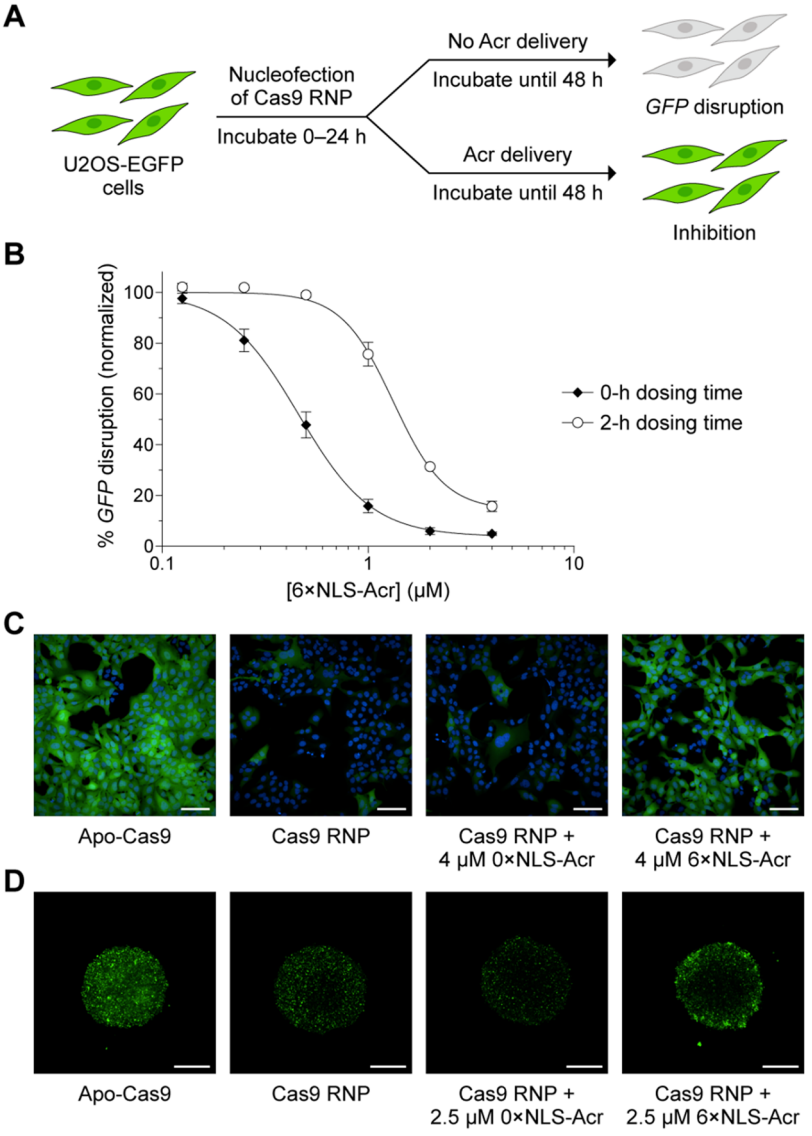


Figure 2. Effect of Acr delivery on *GFP* disruption. (A) A cartoon illustrating the experimental setup for the *GFP*-disruption assay. Acr delivery prevents *GFP* disruption. (B) Dose-dependent inhibition of Cas9 by 6×NLS-Acr in the *GFP*-disruption assay. SpCas9-NLS RNP (20 pmol) targeting *GFP* was delivered via nucleofection into U2OS-EGFP.PEST cells. The cells were seeded, incubated at 37 °C, and treated with 6×NLS-Acr (0.13, 0.25, 0.5, 1, 2, or 4 μM) at 0 or 2 h. After 48 h, live cells were stained with Hoechst 33342 and imaged using high-throughput confocal microscopy. The values were normalized to Cas9 RNP (100%, not shown) and are the mean ± standard deviation (SD) of three independent replicates. Some error bars are too small to visualize. (C) Representative fluorescence images (20× magnification) from the *GFP*-disruption assay described in panel B (2-h dosing time). Controls include nucleofection of Apo-Cas9, nucleofection of Cas9 RNP, and nucleofection of Cas9 RNP followed by treatment with 0×NLS-Acr (4 μM) at 2 h. The cell nucleus was stained with Hoechst 33342 (blue). Scale bars, 100 μm. (D) Representative fluorescence images (5× magnification) from a *GFP*-disruption assay adapted for 3D cell cultures. SpCas9-NLS RNP (20 pmol) targeting *GFP* was delivered via nucleofection into U2OS-EGFP.PEST cells. The cells were seeded in a spheroid plate, incubated at 37 °C, and treated with 6×NLS-Acr (2.5 μM) at 7 h. After 48 h, live cells were imaged using high-throughput confocal microscopy. Controls include nucleofection of Apo-Cas9, nucleofection of Cas9 RNP, and nucleofection of Cas9 RNP followed by treatment with 0×NLS-Acr (2.5 μM) at 7 h. Scale bars, 500 μm.

μM) did not inhibit Cas9, indicating that multiple NLS tags are required to mediate Acr delivery. 6×NLS-Acr (2–4 μM) inhibited Cas9 but not Cas12a (Figures S10 and S11), validating the target specificity of 6×NLS-Acr. 6×NLS-Acr was nontoxic to U2OS-EGFP.PEST cells at concentrations ranging from 0.13 to 4 μM, but reduced cell viability by 15% at 8 μM (Figure S12). Hence, concentrations ranging from 0.13 to 4 μM were used in subsequent experiments.

6×NLS-Acr Inhibits Cas9 in 3D Cell Cultures

We evaluated 6×NLS-Acr delivery using a *GFP*-disruption assay adapted for three-dimensional (3D) cell cultures.[31] We delivered Cas9 RNP into U2OS-EGFP.PEST cells via nucleofection and seeded them in a spheroid plate. The cells were then treated with Acrs at 7 and 13 h. Fluorescence imaging showed loosely aggregated spheroids at 7 and 13 h with an average diameter of 2.53 and 2.10 mm, respectively (Figures S13 and S14), and well-defined spheroids at 48 h with an average diameter of 1.25 mm (Figure S15). 6×NLS-Acr (2.5 μM) reduced Cas9 activity from 100 to 32% in the outer spheroid region (0.20 mm in depth) and from 100 to 61% when assessing the mean fluorescence of the entire spheroid region (Figures 2D, S15, and S16). 6×NLS-Acr did not reach the inner spheroid

https://doi.org/10.1021/jacs.5c19089
J. Am. Chem. Soc. 2026, 148, 51200−51211

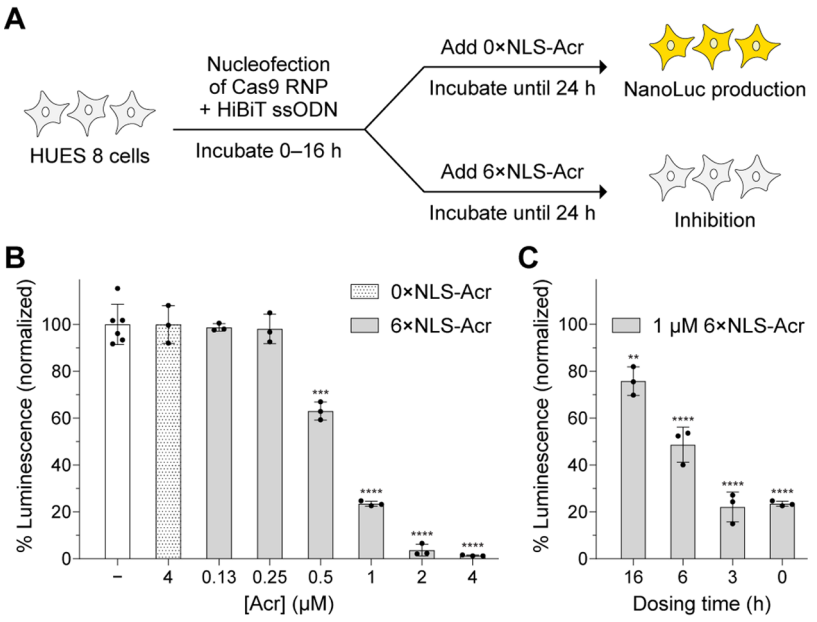


Figure 3. Effect of Acr delivery on HiBiT knock-in. (A) A cartoon illustrating the experimental setup for the HiBiT-knock-in assay. Acr delivery prevents Cas9-mediated knock-in and NanoLuc formation. (B, C) Dose- and time-dependent inhibition of Cas9 by 6×NLS-Acr in the HiBiT-knock-in assay. SpCas9-NLS RNP (20 pmol) targeting *GAPDH* and the HiBiT ssODN (80 pmol) were codelivered via nucleofection into HUES 8 cells. The cells were seeded, incubated at 37 °C, and treated with 6×NLS-Acr (0.13−4 μM) at 0 h (B) or treated with 6×NLS-Acr (1 μM), varying the dosing time from 0−16 h (C). After 24 h, the cells were lysed and combined with LgBiT and furimazine, and their luminescence was quantified. Controls include conucleofection of Cas9 RNP and ssODN (white bar) and conucleofection of Cas9 RNP and ssODN followed by treatment with 4 μM 0×NLS-Acr at 0 h (panel B). The values were normalized to Cas9 RNP with ssODN and are the mean ± SD of three independent replicates. The significance of 6×NLS-Acr delivery was determined using an unpaired, two-tailed *t*-test versus Cas9 RNP with ssODN, where *, **, ***, and **** refer to $P \leq 0.05$, $P \leq 0.01$, $P \leq 0.001$, and $P \leq 0.0001$, respectively.

region. 0×NLS-Acr (2.5 μM) did not inhibit Cas9 in 3D cell cultures.

6×NLS-Acr Inhibits Cas9 in Human Embryonic Stem Cells

We further validated 6×NLS-Acr delivery by monitoring Cas9 nuclease activity using the HiBiT-knock-in assay. We delivered Cas9 RNP targeting *GAPDH* and a HiBiT single-stranded oligodeoxynucleotide (ssODN) donor via nucleofection into human embryonic stem cells (HUES 8). We then treated the seeded cells with Acrs at time points ranging from 0 to 16 h, and quantified luminescence. Cas9-mediated cleavage of *GAPDH* and insertion of the HiBiT ssODN via homology-directed repair (HDR) leads to the formation of NanoLuc in the presence of LgBiT and furimazine. Conversely, inhibition of Cas9 with 6×NLS-Acr prevents NanoLuc formation (Figure 3A). 6×NLS-Acr (0.13−4 μM) inhibited Cas9 activity from 100 to 1.4% (Figure 3B,3C). 0×NLS-Acr (4 μM) did not inhibit Cas9.

We also used the HiBiT-knock-in assay to confirm the delivery of 6×NLS-Acr into HEK293T cells (Figure S17). In addition, we assessed cell viability during the HiBiT-knock-in assay to confirm that 6×NLS-Acr is nontoxic to HUES8 and HEK293T cells (Figures S18 and S19).

Comparing the Delivery of 6×NLS-Acr and LF_N-Acr after Cas9 Nucleofection

Acr delivery was assessed in Cas9-nucleofected cells using the *GFP*-disruption and HiBiT-knock-in assays, which provide functional measurements of delivery effectiveness. Specifically, we define delivery effectiveness as the extent to which the delivered Acr inhibits Cas9 activity. In contrast, delivery efficiency is defined as the ratio of intracellular Acr concentration to the total Acr concentration administered to the well. Delivery effectiveness reflects the functional impact of intracellular Acr and generally increases with delivery efficiency. This relationship is, however, not strictly proportional. Cas9 inhibition can occur even when a small fraction of the administered Acr enters the cell, depending on factors such as Acr potency and the intracellular abundance of Cas9. Potency reflects how effectively the Acr inhibits Cas9 at a given concentration, in this case, the concentration required to reduce Cas9 activity by 50% (IC_{50}). Efficacy is the maximum level of Cas9 inhibition achieved by the Acr and depends on delivery efficiency and effectiveness.

The *GFP*-disruption and HiBiT-knock-in assays confirmed that 6×NLS-Acr effectively enters Cas9-nucleofected cells (Figures 2 and 3). We previously used the same assay conditions to assess PA-mediated delivery of LF_N-Acr.[31] Hence, these assays provide a consistent framework for comparing the delivery effectiveness of different Acrs.

6×NLS-Acr (IC_{50} = 0.47 μM) is 160-fold less potent than the LF_N-Acr/PA system (IC_{50} = 2.9 nM) in the *GFP*-disruption assay (Figure S20 and Table S1). Similarly, 6×NLS-Acr (IC_{50} = 0.63 μM) is 200-fold less potent than the LF_N-Acr/PA system (IC_{50} = 3.1 nM) in the HiBiT-knock-in assay (Figure S21 and Table S1). This effect is expected because PA, a pore-forming protein, mediates the delivery of LF_N-Acr. PA generally delivers cargo more efficiently than CPPs at lower concentrations.[54,55]

6×NLS-Acr inhibited Cas9 more effectively than LF_N-Acr/PA at concentrations above 1 μM in both the *GFP*-disruption (efficacy: 96 versus 86%) and HiBiT-knock-in assays (efficacy: 99 versus 88%) (Table S1). 6×NLS-Acr delivery does not depend on receptors; therefore, its efficiency and effectiveness increase consistently with dose, resulting in higher efficacy. In contrast, LF_N-Acr/PA relies on receptor-mediated uptake that

https://doi.org/10.1021/jacs.5c19089
J. Am. Chem. Soc. 2026, 148, 51200−51211

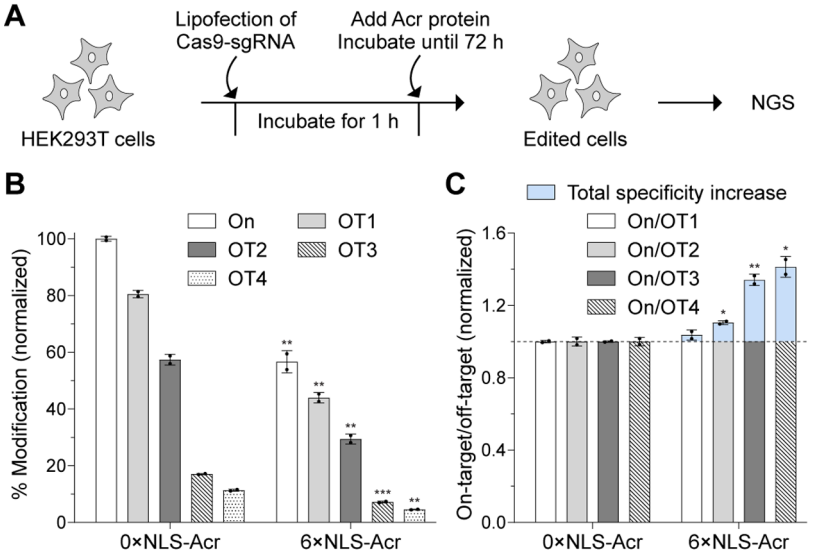


Figure 4. Effect of Acr delivery on genome-editing activity and specificity. (A) A cartoon illustrating the experimental setup for Acr delivery, in which next-generation sequencing (NGS) is used to analyze genome editing. (B) 6×NLS-Acr delivery regulates Cas9 activity. Plasmids encoding 2×NLS-SpCas9 (750 ng) and *EMX1*-targeting gRNA (250 ng) were delivered via lipofection into HEK293T cells. The cells were incubated at 37 °C and treated with 0×NLS-Acr (4 μM, control) or 6×NLS-Acr (4 μM) at 1 h. After 72 h, genomic DNA was extracted, sequenced with NGS, and analyzed using CRISPResso2 to determine the % modification at the on-target (On) and off-target (OT1, OT2, OT3, and OT4) sites. The values were normalized to Cas9·gRNA with 0×NLS-Acr (On) and are the mean ± SD of two independent replicates. The significance of 6×NLS-Acr delivery was determined using an unpaired, two-tailed *t*-test versus Cas9·gRNA with 0×NLS-Acr (separately for On, OT1, OT2, OT3, and OT4), where *, **, ***, and **** refer to $P \leq 0.05$, $P \leq 0.01$, $P \leq 0.001$, and $P \leq 0.0001$, respectively. (C) 6×NLS-Acr delivery increases Cas9 specificity. Specificity was calculated as the ratio of on-target to off-target % modification using data from panel B, normalized to the on-target to off-target % modification ratio of Cas9·gRNA with 0×NLS-Acr (separately for On/OT1, On/OT2, On/OT3, and On/OT4). The significance of the specificity was determined using an unpaired, two-tailed *t*-test compared to the specificity of Cas9·gRNA with 0×NLS-Acr (separately for On/OT1, On/OT2, On/OT3, and On/OT4), where *, **, ***, and **** refer to $P \leq 0.05$, $P \leq 0.01$, $P \leq 0.001$, and $P \leq 0.0001$, respectively. The total specificity increase is shaded in blue.

saturates above 1 μM, likely due to a limited number of PA-targeted receptors on the cell surface.

6×NLS-Acr is the most potent known cell-permeable protein for Cas9 inhibition, whereas LF_N-Acr/PA is the most potent protein-based system. 6×NLS-Acr is the most efficacious Cas9 inhibitor. Depending on the application, either 6×NLS-Acr or LF_N-Acr/PA can be more effective. Thus, these delivery strategies are complementary.

6×NLS-Acr Increases Cas9 Specificity

Delivery of Acrs via nucleofection enhances Cas9 specificity in cells.[22] To determine whether 6×NLS-Acr delivery has a similar effect, we delivered Cas9 and gRNA plasmids via lipid transfection (lipofection) into HEK293T cells, then treated the cells with Acrs. After 72 h, we used next-generation sequencing (NGS) to assess Cas9 cleavage at the *EMX1* on-target and off-target sites (Figure 4A). 6×NLS-Acr (4 μM) reduced Cas9 on-target activity from 100 to 57% and off-target activity from 80 to 44, 57 to 29, 17 to 7.2, and 11 to 4.5% at off-target (OT) sites 1, 2, 3, and 4, respectively (Figure 4B). 6×NLS-Acr increased Cas9 specificity by 1.10- to 1.41-fold (i.e., 10−41%) within each target pair (Figure 4C and eqs S1−S3). Across all target pairs, delivery of 6×NLS-Acr led to a 90% improvement in Cas9 specificity (total specificity increase, eq S4).

Treating cells with LF_N-Acr (250 nM) and PA (20 nM) after Cas9 lipofection did not affect genome-editing activity or specificity (Figure S22). In contrast, treating cells with LF_N-Acr (250 nM) and PA (20 nM) after Cas9 nucleofection inhibited Cas9 and increased its specificity.[31] These contradictory results suggest that lipofection hinders PA-mediated LF_N-Acr delivery.

We also used NGS to assess the activity of a less active Cas9 variant at the *EMX1* site (Figures S23 and S24). These experiments demonstrate that 6×NLS-Acr but not LF_N-Acr/PA enters cells to inhibit Cas9 after lipofection.

6×NLS-Acr Reduces the Local Concentration of DNA-Bound Cas9

We previously developed a platform to study the spatiotemporal dynamics and outcomes of Cas9-mediated genome editing.[56] In this platform, a U2OS cell line stably expressing a Cas9−GFP fusion protein (U2OS-Cas9-GFP cells) is transfected with Ch3Rep gRNA, a truncated gRNA that targets a highly repetitive region on chromosome 3 (Ch3Rep) without inducing its cleavage (Figure 5A). Cas9−GFP in its apo form localizes in the nucleolus. But after pairing with Ch3Rep gRNA, Cas9−GFP accumulates at ∼600 target sites on Ch3Rep, forming distinct nuclear foci observable by fluorescence microscopy (Figure S25). 53BP1−mCherry, also stably expressed in this cell line, serves as a nuclear marker. We adapted this platform to directly visualize Acr-mediated inhibition of Cas9·gRNA in human cells.

We delivered Ch3Rep gRNA via lipofection into U2OS-Cas9-GFP cells. Cells were treated with 6×NLS-Acr (2.5 μM) or LF_N-Acr (2.5 μM) plus PA (20 nM) either 0.5 h before (−0.5 h) or 15 h after (15 h) Ch3Rep gRNA delivery. Pretreating cells with 6×NLS-Acr or LF_N-Acr/PA at −0.5 h prevented the binding of the Cas9−GFP·gRNA complex to Ch3Rep with decreasing effectiveness. 6×NLS-Acr reduced the mean foci intensity, which in turn decreased the percentage of cells with bright foci—those with a mean foci intensity above 2500 au—from 54 to 17% (Figure 5B,5C). LF_N-Acr/PA lowered the mean foci intensity, reducing the percentage of cells with bright foci from 51 to 28%. Most foci were visually faint or undetectable in cells

https://doi.org/10.1021/jacs.5c19089
J. Am. Chem. Soc. 2026, 148, 51200−51211

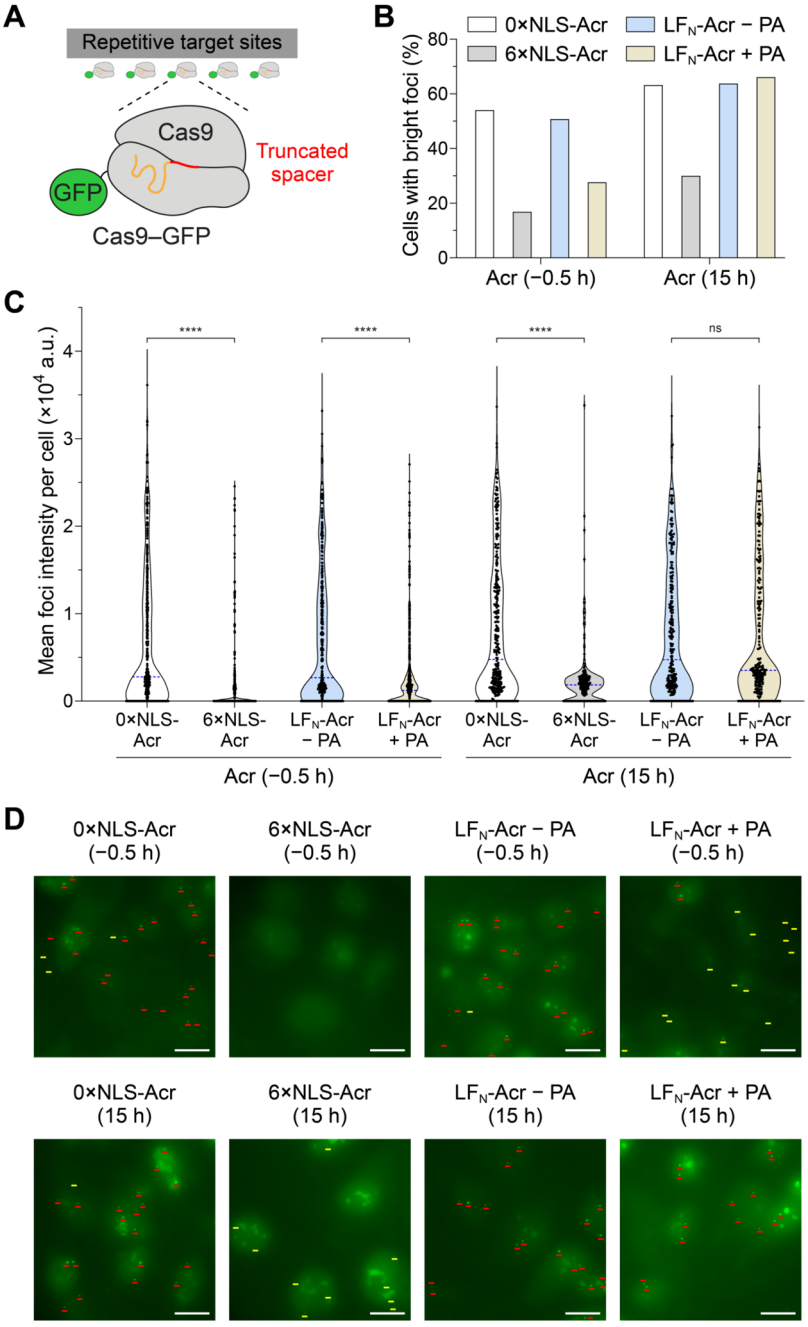


Figure 5. Directly visualizing the Acr-mediated inhibition of fluorescently labeled Cas9. (A) Cas9−GFP complexed with a truncated gRNA targeting a highly repetitive region on chromosome 3 (Ch3Rep) produces nuclear foci in cells. Because the Ch3Rep gRNA spacer is an 11-mer truncation, Cas9−GFP can bind the Ch3Rep target but cannot cleave it. (B, C) Quantifying the inhibition of Cas9−GFP by 6×NLS-Acr and LF_N-Acr. Ch3Rep gRNA was delivered via lipofection into a U2OS cell line stably expressing SpCas9−GFP. Cells were treated with 6×NLS-Acr (2.5 μM) or LF_N-Acr (2.5 μM) plus PA (20 nM) either 0.5 h before (−0.5 h) or 15 h after (15 h) gRNA transfection. Controls include cells treated with 0×NLS-Acr (2.5 μM) or LF_N-Acr (2.5 μM) at −0.5 or 15 h. Live cells were imaged using widefield fluorescence microscopy (60× objective) at 15 and 20 h for −0.5- and 15-h Acr treatments, respectively. Nuclear foci intensity was quantified. Cells with "bright foci" have a mean foci intensity above 2,500 au and are shown as a percentage of total cells in panel B. The mean foci intensity per cell is shown as a violin plot in panel C, with the median of these values indicated by a dashed blue line. The total number of quantified cells per condition was 505, 297, 390, 373, 318, 263, 254, and 233 from left to right. The significance of 6×NLS-Acr and LF_N-Acr/PA delivery was determined using a Mann−Whitney test versus 0×NLS-Acr and LF_N-Acr delivery, respectively. ns, *, **, ***, and **** refer to not significant, $P \leq 0.05$, $P \leq 0.01$, $P \leq 0.001$, and $P \leq 0.0001$, respectively. (D) Representative maximum intensity projection images from the experiment described in panels B and C. Visually bright foci are marked with red lines, and visually faint foci with yellow lines. This classification is qualitative and not based on quantitative measurements; therefore, the terms "visually bright" and "visually faint" are used instead. Scale bars, 20 μm.

pretreated with LF_N-Acr/PA or 6×NLS-Acr, respectively (Figures 5D and S25). Treating cells with 6×NLS-Acr at 15 h reduced the binding of the Cas9−GFP·gRNA complex at Ch3Rep, lowering the mean foci intensity and percentage of cells with bright foci from 63 to 30% (Figure 5B,5C). Foci were visually faint after treating cells with 6×NLS-Acr at 15 h (Figures

https://doi.org/10.1021/jacs.5c19089
J. Am. Chem. Soc. 2026, 148, 51200−51211

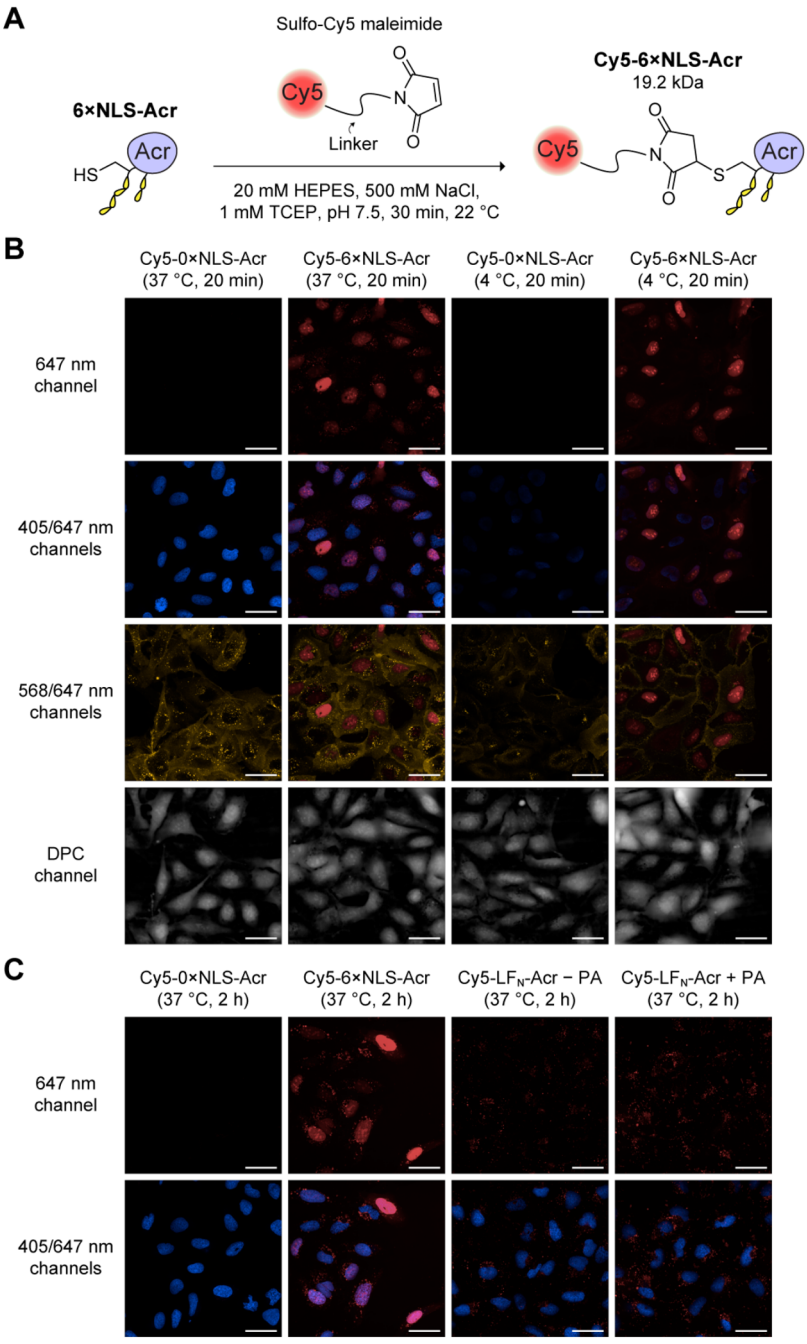


Figure 6. Visualizing the delivery of fluorescently labeled Acrs. (A) Synthesis of Cy5-6×NLS-Acr. 6×NLS-Acr was reacted with sulfo-Cyanine5 (sulfo-Cy5) maleimide to generate Cy5-6×NLS-Acr. (B, C) U2OS cells were seeded and incubated overnight at 37 °C. Cells were then treated with Cy5-0×NLS-Acr (1.5 μM), Cy5-6×NLS-Acr (1.5 μM), or Cy5-LF_N-Acr (2.5 μM) ± PA (20 nM), and incubated either for 20 min at 37 or 4 °C (panel B) or for 2 h at 37 °C (panel C). Cells were washed and stained with Hoechst 33342 and WGA555 in FluoroBrite DMEM, then imaged using confocal microscopy (60× objective) to detect fluorescence from Hoechst 33342 (blue nuclear marker; 405 nm excitation), WGA555 (yellow cell membrane marker; 568 nm excitation), and Cy5 (red; 647 nm excitation). Digital phase contrast (DPC) microscopy was also performed. Scale bars, 40 μm.

5D and S25). Treatment with LF_N-Acr/PA at 15 h failed to inhibit the Cas9−GFP·gRNA complex, confirming that lipofection reagents interfere with PA-mediated Acr delivery.

Comparing the Delivery of 6×NLS-Acr and LF_N-Acr after Cas9 and gRNA Lipofection

6×NLS-Acr effectively entered cells after Cas9 and gRNA lipofection (Figures 4, 5, S23, and S25). In contrast, PA-mediated LF_N-Acr delivery was undetectable after Cas9 and gRNA lipofection (Figures 5, S22, S24, and S25). A possible explanation for these results is that lipofection reagents can shield the cellular receptors required for PA pore formation and subsequent LF_N-Acr uptake. Therefore, the one-component nature and receptor-independent delivery mechanism of 6×NLS-Acr are advantageous when Acr delivery follows Cas9 or gRNA lipofection.

https://doi.org/10.1021/jacs.5c19089
J. Am. Chem. Soc. 2026, 148, 51200−51211

6×NLS-Acr Enters Cells via a Non-Endocytic Direct Delivery Mechanism

To directly visualize Acr delivery and assess its efficiency, we conjugated 0×NLS-Acr and 6×NLS-Acr to a Cy5 dye via thiol−maleimide chemistry (Figures 6A and S26). We then incubated U2OS cells and INS-1E rat β-cells with Cy5-0×NLS-Acr (1−4 μM) or Cy5-6×NLS-Acr (1−4 μM) and visualized Acr uptake by confocal microscopy at time points ranging from 5 min to 2 h. Cy5-6×NLS-Acr fluorescence was predominantly diffuse and localized to the nucleus in both cell types (Figures 6B and S27−S29). Discrete cytoplasmic puncta were observed in a small subset of cells, suggesting that while endocytic uptake occurs, it is largely outcompeted by direct cell entry. Cy5-6×NLS-Acr fluorescence increased in a dose-dependent manner (Figure S28). Cellular uptake occurred within the first 5 min (Figure S29). Similar to arginine-rich CPP−protein conjugates that directly transduce cells,[57] Cy5-6×NLS-Acr is often localized to RNA-rich nucleoli, visible as high-intensity, round structures within the nucleus. In contrast, Cy5-0×NLS-Acr uptake was undetectable relative to that of Cy5-6×NLS-Acr, confirming that the 6×NLS tag mediates Acr delivery.

Cy5-6×NLS-Acr exhibited diffuse fluorescence when incubated with cells at 4 °C, a condition that inhibits endocytosis (Figures 6B and S30).[58] Quantification of Cy5 fluorescence intensity in the nucleus (I_N) and cytoplasm (I_C) showed that the nuclear-to-cytoplasmic localization ratio (I_N/I_C) of Cy5-6×NLS-Acr increased slightly at 4 °C (I_N/I_C = 5.6) relative to 37 °C (I_N/I_C = 5.4, Table S2). In a separate experiment, we examined the effects of small-molecule inhibitors of endocytosis.[59] In cells pretreated with either amiloride (a macropinocytosis inhibitor), bafilomycin A1 (an endosomal acidification inhibitor), or water (vehicle control), Cy5-6×NLS-Acr uptake was indistinguishable (Figure S31 and Table S2). But chloroquine (another endosomal acidification inhibitor) increased the nuclear-to-cytoplasmic localization ratio of Cy5-6×NLS-Acr (I_N/I_C = 7.9) relative to the other conditions (I_N/I_C = 2.7−2.9, Table S2). These findings indicate that Cy5-6×NLS-Acr can enter cells via a direct delivery mechanism, a process that is maintained or even enhanced when endocytic pathways are inhibited.

We performed a *GFP*-disruption assay to determine if Cy5-6×NLS-Acr conserves the activity of 6×NLS-Acr. We treated U2OS-EGFP.PEST cells with Cy5-6×NLS-Acr (0.13−4 μM) following Cas9 nucleofection, assessed *GFP* disruption (Figures S32−34), and quantified Cy5 intensity after 30 h (Figure S35 and Table S2). Cy5-6×NLS-Acr (IC_{50} = 0.67 μM) and 6×NLS-Acr (IC_{50} = 0.56 μM) exhibited comparable potency (Figure S32 and Table S1). But after 30 h of incubation, Cy5-6×NLS-Acr fluorescence was punctate and predominantly cytoplasmic (I_N/I_C = 0.42−0.86; Figure S35 and Table S2), the opposite of the trend observed after 5 min to 2 h of incubation (Figures 6 and S27−S31).

For comparison, we synthesized Cy5-LF_N-Acr and visualized its PA-mediated delivery using confocal microscopy (Figures 6C, S36, and S37). Cy5-LF_N-Acr fluorescence appeared as discrete cytoplasmic puncta regardless of PA addition, consistent with endosomal entrapment. The fluorescence intensity of Cy5-LF_N-Acr (2.5 μM) alone was slightly lower than in cells cotreated with Cy5-LF_N-Acr (2.5 μM) and PA (20 nM), but the localization pattern remained indistinguishable and predominantly cytoplasmic (I_N/I_C = 0.65, Table S2). These results suggest that Cy5-LF_N-Acr translocation to the cytosol via the PA pore is minimal and near the detection threshold of confocal microscopy, or alternatively, that the Cy5 dye impedes LF_N-Acr translocation through the PA pore. To distinguish between these two possibilities, we cotreated U2OS-EGFP.PEST cells with Cy5-LF_N-Acr (0.5−2.5 μM) and PA (20 nM) following Cas9 nucleofection. We then assessed *GFP* disruption (Figures S38 and S39) and directly visualized LF_N-Acr delivery using the Cy5 tag (Figure S40). Cy5-LF_N-Acr inhibited Cas9 activity in the presence of PA but not when administered alone. Consistently, Cy5-LF_N-Acr fluorescence intensity and localization in cells remained nearly indistinguishable regardless of PA addition (I_N/I_C = 0.56−0.59 or 0.79−0.80; Figure S40 and Table S2). Thus, Cy5-LF_N-Acr translocates through the PA pore, but its cellular concentration is below the detection limit of confocal microscopy or overshadowed by endosomally entrapped Cy5-LF_N-Acr. Together, these findings indicate that 6×NLS-Acr delivery is more efficient than PA-mediated delivery of LF_N-Acr above 1 μM, due to its ability to achieve higher intracellular Acr concentrations.

■ DISCUSSION

We introduce 6×NLS-Acr—the first cell-permeable anti-CRISPR protein—and its application to regulating CRISPR-Cas9 activity and specificity. 6×NLS-Acr enters cells within 5 min, reaching higher intracellular concentrations and inhibiting Cas9 with higher efficacy than LF_N-Acr/PA, the most potent protein-based anti-CRISPR delivery system. Therefore, 6×NLS-Acr is the most efficacious cell-permeable Cas9 inhibitor.

We used molecular cloning to engineer 6×NLS-Acr, then produced and purified it as a recombinant protein. We selected a 6×NLS tag because six NLSs are required to shift the p*I* of AcrIIA4, which is a highly anionic, non−cell-permeable protein, from 4.2 to 9.9, thereby matching the p*I* range of model cell-permeable proteins studied in our laboratory (p*I* 9−10).[60,61] Moreover, compared with other NLS tag configurations, a 6×NLS fusion has been reported to deliver Cas9 RNP most effectively into cells.[47] Notably, constructs bearing 2 to 5 NLSs can also mediate intracellular delivery of zinc finger nucleases and Cas9 RNP,[46,47] suggesting that AcrIIA4 fused to fewer NLS motifs may retain partial cell permeability. Our ongoing studies aim to identify the minimal number of NLSs required for effective Acr delivery. Furthermore, the engineered cysteine residue enables site-specific Acr conjugation, providing a modular strategy for adding NLSs and other moieties (e.g., cleavable tags).[62,63]

6×NLS-Acr inhibited Cas9 in spheroid-like 3D cell aggregates. We assessed 6×NLS-Acr delivery in a loosely aggregated spheroid model because spheroids exhibit diffusional limitations similar to those of in vivo tissues.[64] 6×NLS-Acr inhibited Cas9 within the outer 200 μm region of the spheroid with effectiveness comparable to that of LF_N-Acr/PA.[31] The observed decrease in GFP intensity with spheroid depth (Figures 2D, S15, and S16) indicates limited penetration of 6×NLS-Acr into the inner region. A similar trend was observed for LF_N-Acr/PA because diffusion restricts the penetration of molecules to the outer layers of spheroids (50−200 μm in depth).[31,64] This diffusion barrier may also limit distribution in vivo, particularly in poorly vascularized tumor regions, and should be considered when evaluating translational potential.

6×NLS-Acr inhibited Cas9 in a dose- and time-dependent manner in embryonic stem cells (Figure 3B,3C). 6×NLS-Acr inhibited Cas9 more effectively than LF_N-Acr at concentrations above 1 μM, highlighting the potential of 6×NLS-Acr for ex vivo, Acr-based stem cell therapy applications.[25,33,65]

https://doi.org/10.1021/jacs.5c19089
J. Am. Chem. Soc. 2026, 148, 51200−51211

6×NLS-Acr delivery increased Cas9 specificity by up to 41% per off-target site and by 90% when considering multiple off-target sites (Figure 4C). This analysis was, however, limited to four previously reported *EMX1* off-target sites, so the 90% value does not represent genome-wide specificity. We anticipate that genome-wide off-target analyses (e.g., GUIDE-Seq[66]) will reveal the full potential of 6×NLS-Acr. Moreover, milder 6×NLS-Acr variants could be engineered to suppress Cas9 off-target activity selectively, as previously demonstrated with anti-CRISPR vector systems.[29,67,68]

PA-mediated delivery of LF_N-Acr after Cas9 nucleofection increased genome-editing specificity by 40%.[31] Yet, LF_N-Acr delivery after Cas9 lipofection did not affect genome-editing activity or specificity (Figures S22 and S24), likely because lipofection reagents disrupt PA's receptor-dependent protein delivery mechanism. PA effectively mediated delivery of LF_N-Acr prior to gRNA lipofection (Figures 5 and S25), supporting this hypothesis. Further research is needed to understand how lipofection reagents affect PA-mediated protein delivery and whether other lipid-based Cas9 delivery methods (e.g., lipid nanoparticles) interfere with PA's mechanism.

As a one-component system that bypasses receptor-mediated uptake, 6×NLS-Acr is more practical than LF_N-Acr/PA when receptors are inaccessible, for example, when lipofection reagents coat the cell surface. Unlike receptor-dependent systems, 6×NLS-Acr delivery is less prone to saturation. Furthermore, like other CPP-based protein delivery methods,[69,70] 6×NLS-Acr delivery might be effective in bacterial and plant cells that lack the anthrax receptors targeted by LF_N-Acr/PA. Besides delivery applications, the cationic 6×NLS tag could serve as an affinity tag, enabling the adsorption of Acrs to a solid support.[60]

We used 6×NLS-Acr and LF_N-Acr/PA to visualize the inhibition of a fluorescent Cas9−GFP·gRNA complex that binds but does not cleave DNA in cells (Figures 5 and S25). 6×NLS-Acr inhibited Cas9−GFP·gRNA more effectively than LF_N-Acr/PA. Inhibition by 6×NLS-Acr was, however, less pronounced when delivered at 15 h than at −0.5 h, as reflected by a higher percentage of cells with bright foci. Importantly, this increase does not indicate enhanced Cas9−GFP·gRNA binding to DNA, but rather reduced susceptibility of DNA-bound Cas9−GFP·gRNA to Acr-mediated inhibition.

Because AcrIIA4 generally tolerates terminal fusions, we expect 6×NLS-Acr to retain a similar Cas9 inhibition mechanism.[20] Therefore, 6×NLS-Acr likely binds and inhibits Cas9−GFP·gRNA but not Cas9−GFP·gRNA·DNA. By 15 h, most Cas9−GFP·gRNA complexes have engaged their DNA targets; thus, 6×NLS-Acr would inhibit only the complexes that transiently dissociate from DNA (e.g., due to cellular processes), resulting in the observed reduction in activity. In contrast, when delivered at −0.5 h, 6×NLS-Acr prevents Cas9−GFP·gRNA from binding DNA in the first place, leading to more effective inhibition and fewer cells with foci.

LF_N-Acr/PA did not inhibit Cas9−GFP·gRNA when delivered at 15 h, likely because lipofection reagents impaired its cellular entry. In contrast, our previous CRISPRa experiments showed that PA-mediated delivery of LF_N-Acr at 12 h can inhibit DNA binding by nucleofected dCas9.[31]

Plasmids expressing Acrs were previously used to visualize the inhibition of a fluorescent dCas9 system in cells.[17,71,72] Similarly, 6×NLS-Acr produced a comparable inhibitory effect on the DNA-binding activity of Cas9−GFP·gRNA without requiring plasmid-based Acr expression. In both experiments, inhibition of the fluorescent Cas9 system resulted in diminished foci intensity and elevated background fluorescence.

Our work also established a site-specific Acr conjugation platform. Conjugation of 6×NLS-Acr to a fluorescent dye enabled visualization and elucidation of its delivery mechanism (Figures 6 and S26−S31 and Table S2). 6×NLS-Acr entered cells within 5 min, primarily via direct cytosolic uptake, with minimal endocytic entrapment. 6×NLS-Acr achieved intracellular concentrations much higher than LF_N-Acr, highlighting the advantage of a receptor-independent delivery mechanism (Figure 6C).

To characterize the intracellular distribution of Cy5-6×NLS-Acr, we quantified the nuclear-to-cytoplasmic Cy5 intensity ratio (I_N/I_C, Table S2). I_N/I_C provides an internally normalized metric that minimizes variability between replicates. Cy5-6×NLS-Acr was enriched in the nucleus by 3.5- to 5.4-fold when incubating for 5 min to 2 h.

Suppressing endocytic pathways by lowering the incubation temperature to 4 °C or by using small-molecule inhibitors did not reduce the nuclear localization of 6×NLS-Acr (Figures 6B, S30, and S31, and Table S2). Consistent with this observation, previous reports indicate that reducing the temperature to 4 °C does not impair cellular uptake of the SV40 NLS peptide.[73] Further, pretreating cells with chloroquine enhanced the nuclear localization of 6×NLS-Acr by 2.8-fold (I_N/I_C = 7.9) compared with water pretreatment (I_N/I_C = 2.8, Table S2). In addition to inhibiting endosomal acidification, chloroquine acts as an enhancer of endosomal escape—a property that has been used to improve NLS-mediated gene delivery.[74,75] Thus, chloroquine likely promotes endosomal escape in the small fraction of endocytosed 6×NLS-Acr.

In contrast, at 30 h post-treatment in the *GFP* disruption assay, Cy5-6×NLS-Acr fluorescence was approximately 1.2- to 2.4-fold higher in the cytoplasm than in the nucleus (I_N/I_C = 0.42−0.86; Figure S35 and Table S2). This redistribution of fluorescence could result from proteasomal degradation of Cy5-6×NLS-Acr, leaving the residualizing, anionic Sulfo-Cy5 dye to accumulate in the cytoplasm.[76,77]

Cy5-LF_N-Acr fluorescence intensity and localization were largely unaffected by PA addition and exhibited approximately 1.3- to 1.8-fold enrichment in the cytoplasm after 2 or 30 h of treatment (I_N/I_C = 0.56−0.80; Figure S40 and Table S2). Further studies will be required to determine the long-term intracellular fate of 6×NLS-Acr and LF_N-Acr and to enable absolute quantification of their intracellular concentrations.

Narrowing the cell entry time of 6×NLS-Acr to ≤5 min has important implications for future studies of Cas9 kinetics and DNA repair. For example, our time-dependent studies using the HiBiT-knock-in assay confirmed that Cas9 RNP remains active for at least 16 h ± 5 min in human embryonic stem cells. By tracking Cas9 and DNA repair dynamics and understanding the time scale of 6×NLS-Acr delivery, we are poised to explore a broader range of fundamental questions in genome biology.

In vivo Acr delivery has been validated in mice without observable toxicity.[27,35] These studies, however, did not determine the safety and immunity profiles of delivered Acrs. Although 6×NLS-Acr delivery could be effective in vivo, some issues require consideration. Cytotoxicity, as observed at 8 μM (Figure S12), and potential immunogenic responses against the 6×NLS tag or Acr could limit the clinical applicability of 6×NLS-Acr. For example, when delivered to mice via intracranial injection, 4×NLS-Cas9-2×NLS RNP caused an immune response, which was lowered by removing endotoxin contam-

https://doi.org/10.1021/jacs.5c19089
J. Am. Chem. Soc. 2026, 148, 51200−51211

ination.[50] In addition, the efficacy of 6×NLS-Acr delivery in vivo can be improved by employing immunosuppressants and screening for pre-existing immunity.[14] Nevertheless, detailed toxicity profiling and dose optimization will be required before in vivo translation.

Without in vivo studies, the tissue specificity of 6×NLS-Acr remains unclear. Still, 6×NLS-Acr could be targetable to neurons via intracranial injection, as demonstrated previously with cell-permeable NLS-Cas9 variants.[47,50,51] Additionally, we can conjugate cell-targeting ligands to 6×NLS-Acr to improve its tissue specificity.[78] Ongoing work aims to define the effective dose, immunogenicity, and tissue specificity of 6×NLS-Acr in vivo to support its development as a cotherapy for therapeutic genome editing.

■ CONCLUSION

We established the first peptide-based delivery method for introducing Acrs into human cells. 6×NLS-Acr is the most potent cell-permeable anti-CRISPR protein identified to date and enters cells via direct protein transduction. It effectively inhibits Cas9 in stem cell and 3D cultures, enhancing genome-editing specificity by nearly 100%. 6×NLS-Acr holds promise for studying the dynamics of genome editing and for reducing off-target effects, both ex vivo and in vivo, potentially improving the safety and efficacy of therapeutic genome editing.

■ ASSOCIATED CONTENT

Supporting Information

The Supporting Information is available free of charge at https://pubs.acs.org/doi/10.1021/jacs.5c19089. Experimental methods; production, purification, and bioconjugation of Acrs; additional data from the *GFP*-disruption, HiBiT-knock-in, NGS, Cas9−GFP (Ch3Rep), and Cy5-Acr assays; cell viability after Acr delivery; compilation of IC_{50}, efficacy, and I_N/I_C values; cell lines and nucleic acid sequences (plasmid, gRNA, ssODN, primer, and amplicon sequences)

■ AUTHOR INFORMATION

Corresponding Authors

Amit Choudhary − *Chemical Biology and Therapeutics Science Program, Broad Institute of MIT and Harvard, Cambridge, Massachusetts 02142, United States; Divisions of Renal Medicine and Engineering, Brigham and Women's Hospital, Boston, Massachusetts 02115, United States; Department of Medicine, Harvard Medical School, Boston, Massachusetts 02115, United States;* orcid.org/0000-0002-8437-0150; Email: achoudhary@bwh.harvard.edu

Ronald T. Raines − *Department of Chemistry and Koch Institute for Integrative Cancer Research, Massachusetts Institute of Technology, Cambridge, Massachusetts 02139, United States; Chemical Biology and Therapeutics Science Program, Broad Institute of MIT and Harvard, Cambridge, Massachusetts 02142, United States;* orcid.org/0000-0001-7164-1719; Email: rtraines@mit.edu

Authors

Axel O. Vera − *Department of Chemistry, Massachusetts Institute of Technology, Cambridge, Massachusetts 02139, United States; Chemical Biology and Therapeutics Science Program, Broad Institute of MIT and Harvard, Cambridge, Massachusetts 02142, United States;* orcid.org/0000-0003-4522-2793

Franklin J. Avilés-Vázquez − *Howard Hughes Medical Institute and Program in Cellular and Molecular Medicine, Boston Children's Hospital, Boston, Massachusetts 02115, United States; Department of Biophysics and Biophysical Chemistry, Johns Hopkins University, Baltimore, Maryland 21218, United States*

Taekjip Ha − *Howard Hughes Medical Institute and Program in Cellular and Molecular Medicine, Boston Children's Hospital, Boston, Massachusetts 02115, United States; Department of Pediatrics, Harvard Medical School, Boston, Massachusetts 02115, United States;* orcid.org/0000-0003-2195-6258

Complete contact information is available at: https://pubs.acs.org/10.1021/jacs.5c19089

Funding

A.O.V. was supported by an MIT Dean of Science Fellowship, an NIH predoctoral fellowship (F31 GM148042), and an HHMI Gilliam fellowship (GT15945). Cell imaging was performed with an Opera Phenix High-Throughput imaging system that was supported by Grant S10 OD026839 (NIH). This work was supported by Grants R01 GM137606, R35 GM148220, R35 GM122569, and U01 DK127432 (NIH), and by the Merkin Institute of Transformative Technologies in Healthcare.

Notes

The authors declare the following competing financial interest(s): The Broad Institute of MIT and Harvard has filed patent applications claiming the invention of genome editing methods described in this manuscript. Inventors: A.O.V., A.C., and R.T.R.

■ ACKNOWLEDGMENTS

The authors thank Dr. Santosh Chaudhary (Broad Institute of MIT and Harvard) for providing a plasmid for the bacterial production and purification of wild-type AcrIIA4 and sharing his purification method, Michael C. Stark (Broad Institute of MIT and Harvard) for acquiring HUES 8 cells for our laboratory and providing INS-1E rat β-cells for Figure S28, and Prof. J. Keith Joung (Harvard Medical School) for providing the U2OS-EGFP.PEST cell line.

■ REFERENCES

(1) Barrangou, R.; Fremaux, C.; Deveau, H.; Richards, M.; Boyaval, P.; Moineau, S.; Romero, D. A.; Horvath, P. CRISPR provides acquired resistance against viruses in prokaryotes. *Science* **2007**, *315*, 1709−1712.

(2) Jinek, M.; Chylinski, K.; Fonfara, I.; Hauer, M.; Doudna, J. A.; Charpentier, E. A programmable dual-RNA−guided DNA endonuclease in adaptive bacterial immunity. *Science* **2012**, *337*, 816−821.

(3) Cong, L.; Ran, F. A.; Cox, D.; Lin, S.; Barretto, R.; Habib, N.; Hsu, P. D.; Wu, X.; Jiang, W.; Marraffini, L. A.; Zhang, F. Multiplex genome engineering using CRISPR/Cas systems. *Science* **2013**, *339*, 819−823.

(4) Mali, P.; Yang, L.; Esvelt, K. M.; Aach, J.; Guell, M.; DiCarlo, J. E.; Norville, J. E.; Church, G. M. RNA-guided human genome engineering via Cas9. *Science* **2013**, *339*, 823−826.

(5) Frangoul, H.; Altshuler, D.; Cappellini, M. D.; Chen, Y.-S.; Domm, J.; Eustace, B. K.; Foell, J.; de la Fuente, J.; Grupp, S.; Handgretinger, R.; Ho, T. W.; Kattamis, A.; Kernytsky, A.; Lekstrom-Himes, J.; Li, A. M.; Locatelli, F.; Mapara, M. Y.; de Montalembert, M.; Rondelli, D.; Sharma, A.; Sheth, S.; Soni, S.; Steinberg, M. H.; Wall, D.; Yen, A.; Corbacioglu, S. CRISPR-Cas9 gene editing for sickle cell disease and β-thalassemia. *N. Engl. J. Med.* **2021**, *384*, 252−260.

(6) Gillmore, J. D.; Gane, E.; Taubel, J.; Kao, J.; Fontana, M.; Maitland, M. L.; Seitzer, J.; O'Connell, D.; Walsh, K. R.; Wood, K.; Phillips, J.; Xu, Y.; Amaral, A.; Boyd, A. P.; Cehelsky, J. E.; McKee, M. D.; Schiermeier, A.; Harari, O.; Murphy, A.; Kyratsous, C. A.; Zambrowicz, B.; Soltys, R.; Gutstein, D. E.; Leonard, J.; Sepp-Lorenzino, L.; Lebwohl, D. CRISPR-Cas9 in vivo gene editing for transthyretin amyloidosis. *N. Engl. J. Med.* **2021**, *385*, 493−502.
(7) Chiesa, R.; Georgiadis, C.; Syed, F.; Zhan, H.; Etuk, A.; Gkazi, S. A.; Preece, R.; Ottaviano, G.; Braybrook, T.; Chu, J.; Kubat, A.; Adams, S.; Thomas, R.; Gilmour, K.; O'Connor, D.; Vora, A.; Qasim, W. Base-edited CAR7 T cells for relapsed T-cell acute lymphoblastic leukemia. *N. Engl. J. Med.* **2023**, *389*, 899−910.
(8) Fu, Y.; Foden, J. A.; Khayter, C.; Maeder, M. L.; Reyon, D.; Joung, J. K.; Sander, J. D. High-frequency off-target mutagenesis induced by CRISPR-Cas nucleases in human cells. *Nat. Biotechnol.* **2013**, *31*, 822−826.
(9) Zuo, E.; Sun, Y.; Wei, W.; Yuan, T.; Ying, W.; Sun, H.; Yuan, L.; Steinmetz, L. M.; Li, Y.; Yang, H. Cytosine base editor generates substantial off-target single-nucleotide variants in mouse embryos. *Science* **2019**, *364*, 289−292.
(10) Liang, S.-Q.; Liu, P.; Ponnienselvan, K.; Suresh, S.; Chen, Z.; Kramme, C.; Chatterjee, P.; Zhu, L. J.; Sontheimer, E. J.; Xue, W.; Wolfe, S. A. Genome-wide profiling of prime editor off-target sites in vitro and in vivo using PE-tag. *Nat. Methods* **2023**, *20*, 898−907.
(11) Guo, C.; Ma, X.; Gao, F.; Guo, Y. Off-target effects in CRISPR/Cas9 gene editing. *Front. Bioeng. Biotechnol.* **2023**, *11*, No. 1143157.
(12) Mehravar, M.; Shirazi, A.; Nazari, M.; Banan, M. Mosaicism in CRISPR/Cas9-mediated genome editing. *Dev. Biol.* **2019**, *445*, 156−162.
(13) Zuccaro, M. V.; Xu, J.; Mitchell, C.; Marin, D.; Zimmerman, R.; Rana, B.; Weinstein, E.; King, R. T.; Palmerola, K. L.; Smith, M. E.; Tsang, S. H.; Goland, R.; Jasin, M.; Lobo, R.; Treff, N.; Egli, D. Allele-specific chromosome removal after Cas9 cleavage in human embryos. *Cell* **2020**, *183*, 1650−1664.
(14) Ewaisha, R.; Anderson, K. S. Immunogenicity of CRISPR therapeutics—critical considerations for clinical translation. *Front. Bioeng. Biotechnol.* **2023**, *11*, No. 1138596.
(15) Haapaniemi, E.; Botla, S.; Persson, J.; Schmierer, B.; Taipale, J. CRISPR-Cas9 genome editing induces a p53-mediated DNA damage response. *Nat. Med.* **2018**, *24*, 927−930.
(16) Fiumara, M.; Ferrari, S.; Omer-Javed, A.; Beretta, S.; Albano, L.; Canarutto, D.; Varesi, A.; Gaddoni, C.; Brombin, C.; Cugnata, F.; Zonari, E.; Naldini, M. M.; Barcella, M.; Gentner, B.; Merelli, I.; Naldini, L. Genotoxic effects of base and prime editing in human hematopoietic stem cells. *Nat. Biotechnol.* **2024**, *42*, 877−891.
(17) Pawluk, A.; Amrani, N.; Zhang, Y.; Garcia, B.; Hidalgo-Reyes, Y.; Lee, J.; Edraki, A.; Shah, M.; Sontheimer, E. J.; Maxwell, K. L.; Davidson, A. R. Naturally occurring off-switches for CRISPR-Cas9. *Cell* **2016**, *167*, 1829−1838.
(18) Rauch, B. J.; Silvis, M. R.; Hultquist, J. F.; Waters, C. S.; McGregor, M. J.; Krogan, N. J.; Bondy-Denomy, J. Inhibition of CRISPR-Cas9 with bacteriophage proteins. *Cell* **2017**, *168*, 150−158.
(19) Hwang, S.; Maxwell, K. L. Diverse mechanisms of CRISPR-Cas9 inhibition by type II anti-CRISPR proteins. *J. Mol. Biol.* **2023**, *435*, No. 168041.
(20) Yang, H.; Patel, D. J. Inhibition mechanism of an anti-CRISPR suppressor AcrIIA4 targeting SpyCas9. *Mol. Cell* **2017**, *67*, 117−127.
(21) Dong, D.; Guo, M.; Wang, S.; Zhu, Y.; Wang, S.; Xiong, Z.; Yang, J.; Xu, Z.; Huang, Z. Structural basis of CRISPR-SpyCas9 inhibition by an anti-CRISPR protein. *Nature* **2017**, *546*, 436−439.
(22) Shin, J.; Jiang, F.; Liu, J.-J.; Bray, N. L.; Rauch, B. J.; Baik, S. H.; Nogales, E.; Bondy-Denomy, J.; Corn, J. E.; Doudna, J. A. Disabling Cas9 by an anti-CRISPR DNA mimic. *Sci. Adv.* **2017**, *3*, No. e1701620.
(23) Kraus, C.; Sontheimer, E. J. Applications of anti-CRISPR proteins in genome editing and biotechnology. *J. Mol. Biol.* **2023**, *435*, No. 168120.
(24) Gebhardt, C. M.; Niopek, D. Anti-CRISPR Proteins and Their Application to Control CRISPR Effectors in Mammalian Systems. In *Mammalian Synthetic Systems*; Ceroni, F.; Polizzi, K., Eds.; Springer US: New York, 2024; pp 205−231.
(25) Li, C.; Psatha, N.; Gil, S.; Wang, H.; Papayannopoulou, T.; Lieber, A. HDAd5/35^{+2} adenovirus vector expressing anti-CRISPR peptides decreases CRISPR/Cas9 toxicity in human hematopoietic stem cells. *Mol. Ther. Methods Clin. Dev.* **2018**, *9*, 390−401.
(26) Matsumoto, D.; Tamamura, H.; Nomura, W. A cell cycle-dependent CRISPR-Cas9 activation system based on an anti-CRISPR protein shows improved genome editing accuracy. *Commun. Biol.* **2020**, *3*, No. 601.
(27) Lee, J.; Mou, H.; Ibraheim, R.; Liang, S.-Q.; Liu, P.; Xue, W.; Sontheimer, E. J. Tissue-restricted genome editing in vivo specified by microRNA-repressible anti-CRISPR proteins. *RNA* **2019**, *25*, 1421−1431.
(28) Hoffmann, M. D.; Aschenbrenner, S.; Grosse, S.; Rapti, K.; Domenger, C.; Fakhiri, J.; Mastel, M.; Börner, K.; Eils, R.; Grimm, D.; Niopek, D. Cell-specific CRISPR-Cas9 activation by microRNA-dependent expression of anti-CRISPR proteins. *Nucleic Acids Res.* **2019**, *47*, No. e75.
(29) Aschenbrenner, S.; Kallenberger, S. M.; Hoffmann, M. D.; Huck, A.; Eils, R.; Niopek, D. Coupling Cas9 to artificial inhibitory domains enhances CRISPR-Cas9 target specificity. *Sci. Adv.* **2020**, *6*, No. eaay0187.
(30) Jain, S.; Xun, G.; Abesteh, S.; Ho, S.; Lingamaneni, M.; Martin, T. A.; Tasan, I.; Yang, C.; Zhao, H. Precise regulation of Cas9-mediated genome engineering by anti-CRISPR-based inducible CRISPR controllers. *ACS Synth. Biol.* **2021**, *10*, 1320−1327.
(31) Vera, A. O.; Truex, N. L.; Sreekanth, V.; Pentelute, B. L.; Choudhary, A.; Raines, R. T. Protective antigen−mediated delivery of an anti-CRISPR protein for precision genome editing. *Proc. Natl. Acad. Sci. U.S.A.* **2025**, *122*, No. e2426960122.
(32) Bubeck, F.; Hoffmann, M. D.; Harteveld, Z.; Aschenbrenner, S.; Bietz, A.; Waldhauer, M. C.; Börner, K.; Fakhiri, J.; Schmelas, C.; Dietz, L.; Grimm, D.; Correia, B. E.; Eils, R.; Niopek, D. Engineered anti-CRISPR proteins for optogenetic control of CRISPR-Cas9. *Nat. Methods* **2018**, *15*, 924−927.
(33) Liu, X. S.; Wu, H.; Krzisch, M.; Wu, X.; Graef, J.; Muffat, J.; Hnisz, D.; Li, C. H.; Yuan, B.; Xu, C.; Li, Y.; Vershkov, D.; Cacace, A.; Young, R. A.; Jaenisch, R. Rescue of Fragile X syndrome neurons by DNA methylation editing of the FMR1 gene. *Cell* **2018**, *172*, 979−992.
(34) Nakamura, M.; Srinivasan, P.; Chavez, M.; Carter, M. A.; Dominguez, A. A.; La Russa, M.; Lau, M. B.; Abbott, T. R.; Xu, X.; Zhao, D.; Gao, Y.; Kipniss, N. H.; Smolke, C. D.; Bondy-Denomy, J.; Qi, L. S. Anti-CRISPR-mediated control of gene editing and synthetic circuits in eukaryotic cells. *Nat. Commun.* **2019**, *10*, No. 194.
(35) Beyersdorf, J. P.; Bawage, S.; Iglesias, N.; Peck, H. E.; Hobbs, R. A.; Wroe, J. A.; Zurla, C.; Gersbach, C. A.; Santangelo, P. J. Robust, durable gene activation in vivo via mRNA-encoded activators. *ACS Nano* **2022**, *16*, 5660−5671.
(36) Wang, D.; Zhang, F.; Gao, G. CRISPR-based therapeutic genome editing: Strategies and in vivo delivery by AAV vectors. *Cell* **2020**, *181*, 136−150.
(37) Barkau, C. L.; O'Reilly, D.; Eddington, S. B.; Damha, M. J.; Gagnon, K. T. Small nucleic acids and the path to the clinic for anti-CRISPR. *Biochem. Pharmacol.* **2021**, *189*, No. 114492.
(38) Gangopadhyay, S. A.; Cox, K. J.; Manna, D.; Lim, D.; Maji, B.; Zhou, Q.; Choudhary, A. Precision control of CRISPR-Cas9 using small molecules and light. *Biochemistry* **2019**, *58*, 234−244.
(39) Klimpel, K. R.; Molloy, S. S.; Thomas, G.; Leppla, S. H. Anthrax toxin protective antigen is activated by a cell surface protease with the sequence specificity and catalytic properties of furin. *Proc. Natl. Acad. Sci. U.S.A.* **1992**, *89*, 10277−10281.
(40) Bradley, K. A.; Mogridge, J.; Mourez, M.; Collier, R. J.; Young, J. A. T. Identification of the cellular receptor for anthrax toxin. *Nature* **2001**, *414*, 225−229.
(41) Scobie, H. M.; Rainey, G. J. A.; Bradley, K. A.; Young, J. A. T. Human capillary morphogenesis protein 2 functions as an anthrax toxin receptor. *Proc. Natl. Acad. Sci. U.S.A.* **2003**, *100*, 5170−5174.

https://doi.org/10.1021/jacs.5c19089
J. Am. Chem. Soc. 2026, 148, 51200−51211

(42) Lange, A.; Mills, R. E.; Lange, C. J.; Stewart, M.; Devine, S. E.; Corbett, A. H. Classical nuclear localization signals: Definition, function, and interaction with importin α. *J. Biol. Chem.* **2007**, *282*, 5101−5105.
(43) Kalderon, D.; Roberts, B. L.; Richardson, W. D.; Smith, A. E. A short amino acid sequence able to specify nuclear location. *Cell* **1984**, *39*, 499−509.
(44) Morris, M. C.; Depollier, J.; Mery, J.; Heitz, F.; Divita, G. A peptide carrier for the delivery of biologically active proteins into mammalian cells. *Nat. Biotechnol.* **2001**, *19*, 1173−1176.
(45) Böhmová, E.; Machová, D.; Pechar, M.; Pola, R.; Venclíková, K.; Janoušková, O.; Etrych, T. Cell-penetrating peptides: A useful tool for the delivery of various cargoes into cells. *Physiol. Res.* **2018**, *67*, S267−S279.
(46) Liu, J.; Gaj, T.; Wallen, M. C.; Barbas, C. F. Improved cell-penetrating zinc-finger nuclease proteins for precision genome engineering. *Mol. Ther. Nucleic Acids* **2015**, *4*, No. e232.
(47) Staahl, B. T.; Benekareddy, M.; Coulon-Bainier, C.; Banfal, A. A.; Floor, S. N.; Sabo, J. K.; Urnes, C.; Munares, G. A.; Ghosh, A.; Doudna, J. A. Efficient genome editing in the mouse brain by local delivery of engineered Cas9 ribonucleoprotein complexes. *Nat. Biotechnol.* **2017**, *35*, 431−434.
(48) Lobba, M. J.; Fellmann, C.; Marmelstein, A. M.; Maza, J. C.; Kissman, E. N.; Robinson, S. A.; Staahl, B. T.; Urnes, C.; Lew, R. J.; Mogilevsky, C. S.; Doudna, J. A.; Francis, M. B. Site-specific bioconjugation through enzyme-catalyzed tyrosine-cysteine bond formation. *ACS Cent. Sci.* **2020**, *6*, 1564−1571.
(49) Zhang, Z.; Baxter, A. E.; Ren, D.; Qin, K.; Chen, Z.; Collins, S. M.; Huang, H.; Komar, C. A.; Bailer, P. F.; Parker, J. B.; Blobel, G. A.; Kohli, R. M.; Wherry, E. J.; Berger, S. L.; Shi, J. Efficient engineering of human and mouse primary cells using peptide-assisted genome editing. *Nat. Biotechnol.* **2024**, *42*, 305−315.
(50) Stahl, E. C.; Sabo, J. K.; Kang, M. H.; Allen, R.; Applegate, E.; Kim, S. E.; Kwon, Y.; Seth, A.; Lemus, N.; Salinas-Rios, V.; Soczek, K. M.; Trinidad, M.; Vo, L. T.; Jeans, C.; Wozniak, A.; Morris, T.; Kimberlin, A.; Foti, T.; Savage, D. F.; Doudna, J. A. Genome editing in the mouse brain with minimally immunogenic Cas9 RNPs. *Mol. Ther.* **2023**, *31*, 2422−2438.
(51) Chen, K.; Stahl, E. C.; Kang, M. H.; Xu, B.; Allen, R.; Trinidad, M.; Doudna, J. A. Engineering self-deliverable ribonucleoproteins for genome editing in the brain. *Nat. Commun.* **2024**, *15*, No. 1727.
(52) Johnston, R. K.; Seamon, K. J.; Saada, E. A.; Podlevsky, J. D.; Branda, S. S.; Timlin, J. A.; Harper, J. C. Use of anti-CRISPR protein AcrIIA4 as a capture ligand for CRISPR/Cas9 detection. *Biosens. Bioelectron.* **2019**, *141*, No. 111361.
(53) Reyon, D.; Tsai, S. Q.; Khayter, C.; Foden, J. A.; Sander, J. D.; Joung, J. K. FLASH assembly of TALENs for high-throughput genome editing. *Nat. Biotechnol.* **2012**, *30*, 460−465.
(54) Liao, X.; Rabideau, A. E.; Pentelute, B. L. Delivery of antibody mimics into mammalian cells via anthrax toxin protective antigen. *ChemBioChem* **2014**, *15*, 2458−2466.
(55) Verdurmen, W. P. R.; Mazlami, M.; Plückthun, A. A quantitative comparison of cytosolic delivery via different protein uptake systems. *Sci. Rep.* **2017**, *7*, No. 13194.
(56) Liu, Y.; Zou, R. S.; He, S.; Nihongaki, Y.; Li, X.; Razavi, S.; Wu, B.; Ha, T. Very fast CRISPR on demand. *Science* **2020**, *368*, 1265−1269.
(57) Herce, H. D.; Schumacher, D.; Schneider, A. F. L.; Ludwig, A. K.; Mann, F. A.; Fillies, M.; Kasper, M.-A.; Reinke, S.; Krause, E.; Leonhardt, H.; Cardoso, M. C.; Hackenberger, C. P. R. Cell-permeable nanobodies for targeted immunolabelling and antigen manipulation in living cells. *Nat. Chem.* **2017**, *9*, 762−771.
(58) Weigel, P. H.; Oka, J. A. Temperature dependence of endocytosis mediated by the asialoglycoprotein receptor in isolated rat hepatocytes. Evidence for two potentially rate-limiting steps. *J. Biol. Chem.* **1981**, *256*, 2615−2617.
(59) Luo, H. C.; Li, N.; Yan, L.; Mai, K. J.; Sun, K.; Wang, W.; Lao, G. J.; Yang, C.; Zhang, L. M.; Ren, M. Comparison of the cellular transport mechanism of cationic, star-shaped polymers and liposomes in HaCat cells. *Int. J. Nanomed.* **2017**, *12*, 1085−1096.
(60) Fuchs, S. M.; Raines, R. T. Polyarginine as a multifunctional fusion tag. *Protein Sci.* **2005**, *14*, 1538−1544.
(61) Chao, T.-Y.; Raines, R. T. Mechanism of ribonuclease A endocytosis: Analogies to cell-penetrating peptides. *Biochemistry* **2011**, *50*, 8374−8382.
(62) Schneider, A. F. L.; Wallabregue, A. L. D.; Franz, L.; Hackenberger, C. P. R. Targeted subcellular protein delivery using cleavable cyclic cell-penetrating peptides. *Bioconjugate Chem.* **2019**, *30*, 400−404.
(63) Chen, F.-J.; Gao, J. Fast cysteine bioconjugation chemistry. *Chem. - Eur. J.* **2022**, *28*, No. e202201843.
(64) Mehta, G.; Hsiao, A. Y.; Ingram, M.; Luker, G. D.; Takayama, S. Opportunities and challenges for use of tumor spheroids as models to test drug delivery and efficacy. *J. Controlled Release* **2012**, *164*, 192−204.
(65) Hendriks, D.; Clevers, H.; Artegiani, B. CRISPR-Cas tools and their application in genetic engineering of human stem cells and organoids. *Cell Stem Cell* **2020**, *27*, 705−731.
(66) Tsai, S. Q.; Zheng, Z.; Nguyen, N. T.; Liebers, M.; Topkar, V. V.; Thapar, V.; Wyvekens, N.; Khayter, C.; Iafrate, A. J.; Le, L. P.; Aryee, M. J.; Joung, J. K. GUIDE-seq enables genome-wide profiling of off-target cleavage by CRISPR-Cas nucleases. *Nat. Biotechnol.* **2015**, *33*, 187−197.
(67) Marsiglia, J.; Vaalavirta, K.; Knight, E.; Nakamura, M.; Cong, L.; Hughes, N. W. Computationally guided high-throughput engineering of an anti-CRISPR protein for precise genome editing in human cells. *Cell Rep. Methods* **2024**, *4*, No. 100882.
(68) Sharrar, A.; de Tacca, L. A.; Meacham, Z.; Staples-Ager, J.; Collingwood, T.; Rabuka, D.; Schelle, M. Discovery and engineering of AiEvo2, a novel Cas12a nuclease for human gene editing applications. *J. Biol. Chem.* **2024**, *300*, No. 105685.
(69) Lee, H.-M.; Ren, J.; Tran, K. M.; Jeon, B.-M.; Park, W.-U.; Kim, H.; Lee, K. E.; Oh, Y.; Choi, M.; Kim, D.-S.; Na, D. Identification of efficient prokaryotic cell-penetrating peptides with applications in bacterial biotechnology. *Commun. Biol.* **2021**, *4*, No. 205.
(70) Li, J.; Li, S.; Du, M.; Song, Z.; Han, H. Nuclear delivery of exogenous gene in mature plants using nuclear location signal and cell-penetrating peptide nanocomplex. *ACS Appl. Nano Mater.* **2023**, *6*, 160−170.
(71) Lee, J.; Mir, A.; Edraki, A.; Garcia, B.; Amrani, N.; Lou, H. E.; Gainetdinov, I.; Pawluk, A.; Ibraheim, R.; Gao, X. D.; Liu, P.; Davidson, A. R.; Maxwell, K. L.; Sontheimer, E. J. Potent Cas9 inhibition in bacterial and human cells by AcrIIC4 and AcrIIC5 anti-CRISPR proteins. *mBio* **2018**, *9*, No. e02321−18.
(72) Song, G.; Zhang, F.; Tian, C.; Gao, X.; Zhu, X.; Fan, D.; Tian, Y. Discovery of potent and versatile CRISPR-Cas9 inhibitors engineered for chemically controllable genome editing. *Nucleic Acids Res.* **2022**, *50*, 2836−2853.
(73) Ragin, A. D.; Morgan, R. A.; Chmielewski, J. Cellular import mediated by nuclear localization signal peptide sequences. *Chem. Biol.* **2002**, *9*, 943−948.
(74) Yang, S.; Coles, D. J.; Esposito, A.; Mitchell, D. J.; Toth, I.; Minchin, R. F. Cellular uptake of self-assembled cationic peptide−DNA complexes: Multifunctional role of the enhancer chloroquine. *J. Controlled Release* **2009**, *135*, 159−165.
(75) Hajimolaali, M.; Mohammadian, H.; Torabi, A.; Shirini, A.; Shal, M. K.; Nezhad, H. B.; Iranpour, S.; Eftekhari, R. B.; Dorkoosh, F. Application of chloroquine as an endosomal escape enhancing agent: new frontiers for an old drug. *Expert Opin. Drug Delivery* **2021**, *18*, 877−889.
(76) Cilliers, C.; Liao, J.; Atangcho, L.; Thurber, G. M. Residualization rates of near-infrared dyes for the rational design of molecular imaging agents. *Mol. Imaging Biol.* **2015**, *17*, 757−762.
(77) Nessler, I.; Cilliers, C.; Thurber, G. M. Practical guide for quantification of in vivo degradation rates for therapeutic proteins with single-cell resolution using fluorescence ratio imaging. *Pharmaceutics* **2020**, *12*, No. 132.
(78) Yang, D.; Liu, B.; Sha, H. Advances and prospects of cell-penetrating peptides in tumor immunotherapy. *Sci. Rep.* **2025**, *15*, No. 3392.

https://doi.org/10.1021/jacs.5c19089
J. Am. Chem. Soc. 2026, 148, 51200−51211